Geothermics 64 (2016) 81–95

Contents lists available at ScienceDirect

Geothermics

journal homepage: www.elsevier.com/locate/geothermics

A semi-analytical correlation of thermal-hydraulic-mechanical behavior of fractures and its application to modeling reservoir scale cold water injection problems in enhanced geothermal reservoirs

Shihao Wang [a], Zhaoqin Huang [a,b,*], Yu-Shu Wu [a], Philip H. Winterfeld [a], Luis E. Zerpa [a]

[a] Department of Petroleum Engineering, Colorado School of Mines, Golden, CO, USA
[b] School of Petroleum Engineering, China University of Petroleum, East China, Qingdao, People's Republic of China

ARTICLE INFO

Article history:
Received 6 September 2015
Received in revised form 13 February 2016
Accepted 13 April 2016
Available online 18 May 2016

Keywords:
Fracture aperture change correlation
Cold water injection
Semi-analytical derivation
Enhanced geothermal systems
Numerical reservoir simulation

ABSTRACT

Fractured enhanced geothermal system (EGS) reservoirs are typically sensitive to thermal and mechanical change induced by cold water injection. It has been observed that the permeability at the cold water injector is significantly enhanced. The physical thermal-hydrologic-mechanic (THM) process behind this phenomenon is that, the injection of cold water decreases the temperature of the reservoir rock and causes the matrix block to shrink, resulting in an increase of the fracture aperture and fracture permeability. Therefore, it is of great importance to quantify the effect of thermally induced fracture aperture change to better predict the behavior/performance of EGS reservoirs.

In this work, we develop a novel correlation of the thermal-induced normal change of fracture aperture. The new correlation is based on the analytical solution of the governing displacement equations. Compared to the existing empirical correlations, the new correlation can better describe the physical processes by including the thermal effect on the matrix-fracture deformation. We have verified this correlation with respect to refined simulation results and implemented this correlation in a fully coupled massively parallel geothermal simulator, THM-EGS. We have applied this correlation to study field scale problems with certain parameters from Habanero Field in Copper Basin, Australia. Our results demonstrate that the fracture permeability near the cold water injector could be enhanced 7 times.

1. Introduction

It is widely accepted that fractures are important to geothermal reservoirs. Many types of fractures are sensitive to pressure and stresses, especially the natural fractures that are penetrated by wells or re-activated by hydraulic fractures. Meanwhile, cold water injection can cause the matrix to shrink and the aperture of the surrounding fractures will be thus increased (the thermal unloading process), resulting in an enhancement of permeability at the area that is close to the injector. Such combined thermal-hydro-mechanical effects of injection and production can dramatically change the properties of fractures (Gelet et al., 2012), or even close some of them, resulting in a huge variation in the conductivity (Settari and Mourits, 1998; Settari and Walters, 2001; Jaeger et al., 2009; Wu et al., 2011)

Fractured reservoirs can be modeled by either discrete fracture method (Barenblatt et al., 1960; Warren and Root, 1963). In discrete fracture method, the geometry of the fracture network is explicitly modeled, while in the dual continuum approach, the fracture network and the matrix rock are modeled as two continuum with average pressure and temperature. Discrete fracture method is naturally more accurate by capturing more flux behaviors between the fracture and the matrix rock (Moinfar et al., 2011). However, the characterization of the fracture network highly depends on the accuracy of logging and geostatistical techniques. Dual continuum method, on the other hand, is more convenient to implement. Moreover, multiple porosity methods, such as MINC (Karsten Pruess, 1985), more accurately describe the flow behavior inside the matrix, by further dividing the matrix rock into multiple continuums.

Injectivity increase phenomena near the cold water injector have been widely observed in geothermal reservoirs (Stefansson and V.-đur, 1997; Kaya et al., 2011). In Geyser geothermal field, micro-earthquake events near the cold water injector have also been recorded and studied (Majer and Peterson, 2007; Rutqvist,

* Corresponding author at: Department of Petroleum Engineering, Colorado School of Mines, Golden, CO, USA.
E-mail addresses: huangzhqin@gmail.com, huangzhqin@upc.edu.cn (Z. Huang).

http://dx.doi.org/10.1016/j.geothermics.2016.04.005
0375-6505/

Nomenclature

A	Interface area of a connection (m^2)
a	Exponential parameter for porosity (dimensionless)
b_i	fracture aperture on the ith direction (m)
d^k_β	diffusive coefficient of component k in phase β (m^2/s)
E	Young's modulus (Pa)
F	flux term (m/s)
G	shear modulus (Pa)
g	gravity terms (m/s^2)
h	specific enthalpy (J/kg)
k	component index (dimensionless)Component index (dimensionless)
K_0	Absolute permeability (m^2)
K_r	Relative permeability (dimensionless)
K_R	Formation heat conductivity (W/m K)
K_β	Liquid heat conductivity (W/m K)
L_i	Fracture spacing along the ith direction (m)
M	Accumulation term (kg/m^3 s)
Q	Generation term (kg/m^3 s)
p	Pore pressure (Pa)
Pc	Capillary pressure (Pa)
S	Phase saturation (dimensionless)
T	Temperature (K)
T_f	Fracture temperature (K)
T_m	Matrix temperature (K)
T_{ref}	Reference temperature (K)
Δt	Length of time step (s)
$\vec{u}$	Displacement vector (m)
u_β	Internal energy of phase β (J/kg)
V	Volume (m^3)
x	Mass component (dimensionless)
α	Biot's coefficient (dimensionless)
β	Phase index (dimensionless)
β_T	Linear thermal expansion coefficient (m/m·K)
ε_k	Diagonal strain component (dimensionless)
ε_v	Volumetric strain (dimensionless)
ε_{kk}	Diagonal strain component (dimensionless)
λ	Lame's coefficient (dimensionless)
μ	Viscosity (Pa·s)
$\nu_{max,hor}$	Maximum horizontal stress (Pa)
$\nu_{min,hor}$	Minimum horizontal stress (Pa)
ρ	Density (kg/m^3)
σ'	Effective stress (Pa)
σ_k	Normal stress along the *k*th direction (Pa)
σ_{kk}	Diagonal stress component (Pa)
σ_m	Mean stress (Pa)
σ'_n	Normal effective stress (Pa)
ϕ	Porosity (dimensionless)
τ_0	Intrinsic tortuosity of the rock (dimensionless)
τ_β	Tortuosity correction of phase β (dimensionless)

2008). Such observations could be explained by the shrinkage of rock induced by change of thermal stress field. Specially, in fractured geothermal reservoir, the injected cold water causes the matrix rock to shrink, increasing the fracture aperture. As the fracture permeability is approximately the cubic power of the fracture aperture, the increase of fracture permeability could be considerable.

In this work, we aim to develop a practical fracture aperture correlation to be used in the fully coupled THM simulation of fractured geothermal reservoirs, in order to quantify the thermal stress effect. Our correlation is based on the Navier's displacement equation, combined with the dual-porosity model. Our correlation can be used in the accurate calculation of cold water injectivity as well as the cold front breakthrough time. The correlation is easy to implement in reservoir simulators. It can also be used in existing simulators even without a mechanical simulation module. The details of the derivation of the correlation and its application are described in the following sessions.

2. Literature review

2.1. Dual porosity model

In reservoir simulation, dual porosity model has been widely used to characterize interconnected fracture system. In the dual porosity model, the fractured system is divided into two types of grid blocks, which are the fracture and the matrix. While the fracture system serves as the major flow channel, the matrix blocks play the role as the fluid storage system. The transmissibility between the fracture system and the matrix block is represented by the concept of a 'shape factor'. The flow rate between the matrix and the fracture is calculated using the following equation.

$$q = \sigma \frac{k_m}{\mu} V_m \left(\overline{P}_m - P_f\right) \tag{1.1}$$

In the above equation, V_m is the volume of the matrix block and σ is the shape factor. The shape factor can be determined by analytical or semi-analytical (Barenblatt et al., 1960; Warren and Root, 1963; Kazemi et al., 1976; Gilman and Kazemi, 1983; Chang, 1993; Zimmerman et al., 1993; Lim and Aziz, 1995).

Recent advances in dual porosity model include the extension to thermal flow (van Heel et al., 2008) and multiphase flow (Lu et al., 2008). In this work, we use the dual porosity model to simulate the fluid flow inside the EGS reservoir.

2.2. Fracture aperture correlation

The normal closure of a set of fractures is just the normal displacement of the fracture, and it is directly related to the effective normal stress that is on the fracture planes. There are mainly two types of models, known as the hyperbolic model and the logarithmic model, to correlate the fracture aperture with the effective normal stress. Among the correlations belonging to the hyperbolic model, the Barton-Bandis' correlation (Bandis et al., 1983; Barton et al., 1985; Bandis, 1990)is the most widely used, and it is shown in the following equation,

$$\Delta b = \frac{\Delta \sigma'_n}{k_n - \frac{\Delta \sigma'_n}{\Delta b_{\max}}} \tag{1.2}$$

where σ'_n is the effective normal stress. Δb is the aperture change (closure), while Δb_{max} is the maximum closure. k_n is the stiffness along the normal direction. Evans' model (Evans et al., 1999) is a widely used logarithmic model, as shown in the following equation,

$$\Delta b = -\left(\frac{dk_n}{d\sigma'_n}\right)^{-1} \ln\left(\frac{\sigma'_n}{\sigma'_{ni}}\right) \tag{1.3}$$

where the σ'_{ni} is the reference effective normal stress.

Rutqvist and Tsang (2003) substituted the hyperbolic model into the cubic law of fracture permeability to calculate the transmissibility of the fractures, as shown in the following equation.

$$T = C\left[b_{ni} + \frac{\sigma'_{ni}}{k_{ni}}\left(1 - \frac{\sigma'_{ni}}{\sigma'_n}\right)\right]^3 \tag{1.4}$$

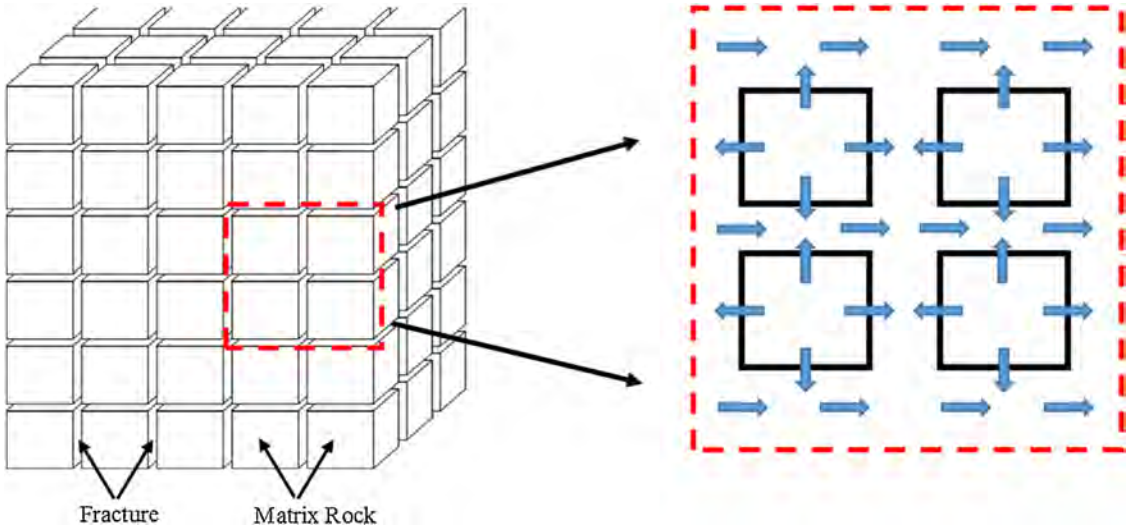

Fig. 1. Conceptual model of dual-porosity model. Left: matrix blocks and fracture system; Right: fluid flow inside the matrix-fracture system.

where K_{ni} and $\sigma_{ni}^{'}$ are the reference normal stiffness and reference effective normal stress respectively, C is an empirical constant. Alm (1999) proposed another equation based on the logarithmic model.

$$T = C\left[b_{ni} - \left(\frac{dk_n}{d\sigma'_n}\right)^{-1} \ln\left(\frac{\sigma'_n}{\sigma'_{ni}}\right)\right]^3 \quad (1.5)$$

As to the fracture behavior in geothermal reservoirs, Ghassemi and Suresh Kumar (2007) have studied the thermal induced aperture change in a 1-D system. In their work, the aperture change of a single fracture within an infinitely large reservoir is calculated and compared with numerical results. Baghbanan and Jing (2007) have investigated the hydraulic properties of fractures in geothermal reservoirs and developed a correlation between hydraulic aperture and fracture length. Berkowitz (1995, 2002) has studied the mechanical behavior using explicitly expressed fracture network model.

The existing models have several limitations. At the first place, most of them are empirical correlations based on uniaxial experimental results with certain fitting parameters. It has been observed that there is scale effect between the fractures in drill core and in-situ condition, as reported by Yoshinaka et al. (1993). The scale effect shows that the normal closure predicted by the drill core test is significantly different from the in-situ normal closure. Secondly, thermal process is not considered in the existing models. Thirdly, the normal effective stress cannot be computed by the mean stress approach. Actually, it is always difficult to exactly capture the normal effective stress on the matrix-fracture interface.

2.3. Coupled THM scheme

The coupling simulation of thermal-hydraulic-mechanical processes in fractured porous media has drawn much attention in recent years (Fung et al., 1994; Wan et al., 2003). As to geothermal reservoir, the development of coupled thermal-hydraulic-mechanical simulator is also a hot research topic. Rutqvist et al. (2002) and Rutqvist and Tsang (2003) coupled the multiphase multicomponent TOUGH2 (Pruess and Oldenburg, 1999) simulator with the geomechanical simulator FLAC3D (Itasca Consulting Group Inc., 1997). In this couple scheme, the displacement calculated by FLAC3D at the corner of each element is converted to stress/strain at the center of the element for the coupling with TOUGH2. This approach has been used to simulate the fracture permeability change induced by thermal loading and unloading in Yucca Mountain heater test (Rutqvist et al., 2005, 2008). Taron et al. (2009) sequentially coupled the multiphase geochemical simulator TOUGHREACT (Xu et al., 2006) with FLAC3D and conducted thermal-hydraulic-mechanical-chemical simulation on geothermal reservoirs. In their work, they investigated the thermal loading and unloading processes on fractured porous media with chemical stress taken into consideration. Kim et al. (2012) developed a sequential coupling approach for the simulation of multiple porosity materials in geothermal reservoirs and conducted stability analysis on it. In their approach, the fluid/heat process and the mechanical process was simulated by finite volume and finite element method respectively. The numerical algorithm is unconditional converged. They also investigated the elastoplastic problem by adopting Mohr-Coulomb failure criteria.

The coupling schemes mentioned above are mostly sequentially or iteratively coupling schemes, in which fluid/heat simulator and mechanical simulator run separately and exchange variable with each time or iteration step. Such schemes are relatively easier to implement. With carefully designed approach, they could be proven to be numerical stable. However, to guarantee the best mass and energy conservation, fully coupled approaches (Fakcharoenphol et al., 2012; Hu et al., 2013) are demanding.

The main objective of this work is to extend the above pioneer research work with analytical and numerical tools to get a more practical approach for the simulation of fractured geothermal reservoirs.

3. Mathematical and numerical approach

3.1. Formulation of fluid and heat flow

We have developed a massively parallel reservoir simulator based on a previous simulator TOUGH-EGS-MP (Wang et al., 2014). The new simulator is called THM-EGS. THM-EGS is a two-phase two-component simulator. The two phases are liquid and gas (vapor) phases, while the two components are air and water components. Each of the two components can exist in either of the two phases. The gas phase is treated as real gas, for which users are allowed to input the gas factor (Z-factor) table. The transition between the liquid and gas phase is determined by comparing the updated system pressure with the saturation pressure of water. More details of the PVT modeling part can be found in (Wang, 2015).

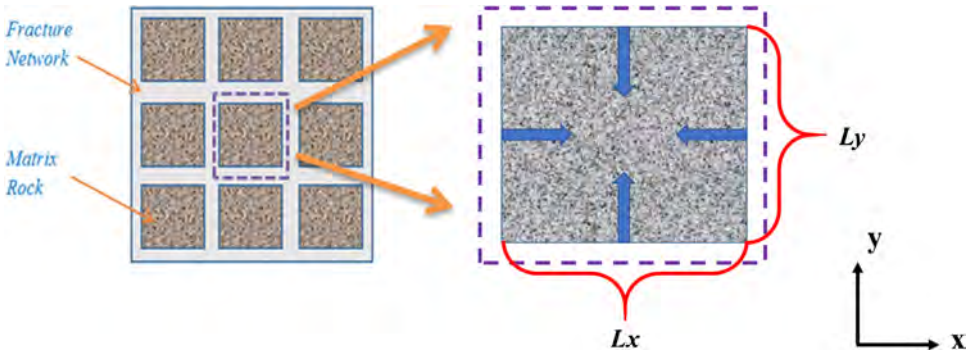

Fig. 2. Conceptual model of fracture surrounded matrix block. The blue arrow denotes the direction of thermal traction (For interpretation of the references to color in this figure legend, the reader is referred to the web version of this article.).

The governing flow equations are build based on the mass conservation of components, and the flux term is calculated from phase flow by Darcy's law.

In THM-EGS the governing equations of mass and heat flow are both in general conservation form, as follows.

$$\frac{dM^k}{dt} = \nabla \times \vec{F}^k + q^k \tag{2.1}$$

in which k refers mass component or heat. In our simulator, k = 1 refers to the water component; k = 2 refers to the air component; k = 3 refers to the heat 'component'.

By integrating the above equation on a representative element volume (REV), we can get the following integrated governing equation,

$$\frac{d}{dt}\int_{V_n} M^k dV_n = \int_{\Gamma_n} \vec{F}^k \times \vec{n} d\Gamma_n + \int_{V_n} q^k dV_n \tag{2.2}$$

In the above equation, $\vec{n}$ is the normal vector on the surface Γ_n, pointing inward to the REV. On the left side of the above equation, the accumulation term of the fluid equation is

$$M^k = \phi \sum_\beta S_\beta \rho_\beta X^k_\beta \tag{2.3}$$

In the above equation, X^k_β is the mass concentration of component k in phase β.

The accumulation term of heat equation can be written in a similar way as follows,

$$M^\kappa = (1-\phi)\rho_R C_R T + \phi \sum_\beta S_\beta \rho_\beta u_\beta \tag{2.4}$$

The accumulation of heat contains two terms. The first term $(1-\phi)\,\rho_R C_R T$ is the energy stored by rock while the second term is the energy stored by fluid. On the right side of Eq. (2.1), the mass flux of liquids consists of advection and diffusion, as shown in Eq. (2.5).

$$\vec{F}^k = \vec{F}^k_{adv} + \vec{F}^k_{dif} \tag{2.5}$$

The advective flux of a component is the sum over all phases:

$$\vec{F}^k = \sum_\beta X^k_\beta \vec{F}_\beta \tag{2.6}$$

where $\vec{F}_\beta$ is given by the multiphase version of Darcy's law;

$$\rightarrow F_\beta = -K_0 \frac{K_{r\beta}\rho_\beta}{\mu_\beta}\left(\nabla P_\beta - \rho_\beta \rightarrow g\right) \tag{2.7}$$

The diffusive mass flux is given by,

$$\rightarrow F^k_{dif} = -\phi\tau_0 \sum_\beta \tau_\beta \rho_\beta d^k_\beta \nabla X^k_\beta \tag{2.8}$$

where the tortuosity τ_0, is an intrinsic property of rock matrix,while the tortuosity τ_β is a property of the fluid. d^k_β is the molecular diffusion coefficient for component κ in phase β. The heat flow includes conduction and convection:

$$\vec{F}^{k=3} = -\left[(1-\phi)K_R + \phi \sum_\beta S_\beta K_\beta\right]\nabla T + \sum_\beta h_\beta \vec{F}_\beta \tag{2.9}$$

where K_R and K_β is thermal conductivity of the rock and the liquid, respectively.

3.2. Formulation of geomechanics module

Recall that the Hooke's law for isothermal elastic materials is as follows,

$$\bar{\bar{\tau}} = 2G\bar{\bar{\varepsilon}} + \lambda(\varepsilon_{xx} + \varepsilon_{yy} + \varepsilon_{zz})\bar{\bar{I}} \tag{2.10}$$

where $\bar{\bar{\tau}}$ is the stress tensor, $\bar{\bar{\varepsilon}}$ is the strain tensor,and $\bar{\bar{I}}$ is a unit tensor.

The above equation has been extended to non-isothermal material by Nowacki (2013) and Norris (1992). Later, the thermoelastic version was extended to poro-thermoelastic version with both pressure and temperature effects by McTigue (1986), as shown in Eq. (2.11).

$$\sigma_{kk} - \left[\alpha P + 3\beta_T K\left(T - T_{ref}\right)\right] = \lambda\varepsilon_v + 2G\varepsilon_{kk}, \quad k = x, y, z \tag{2.11}$$

where ε_v is the volumetric strain, as shown in Eq. (2.12).

$$\varepsilon_v = \varepsilon_{xx} + \varepsilon_{yy} + \varepsilon_{zz} \tag{2.12}$$

THM-EGS assumes the rock to be a linear thermo-poro-elastic material, the behavior of which is subject to Eq. (2.11).

For fractured media, the pore pressure and temperature terms are summed over the multi-porosity continua. We can see from Eq. (2.11) that Lame's constant represents the effects of uniform strain while the shear modulus represent the effects of directional strain. By summing over the x, y and z component of Eq. (2.11) and rewriting it in terms of mean stress and volumetric stain, we get the following equation:

$$\sigma_m - \alpha P - 3\beta_T K\left(T - T_{ref}\right) = \left(\lambda + \frac{2}{3}G\right)\varepsilon_v \tag{2.13}$$

in which

$$\sigma_m = \frac{\sigma_{xx} + \sigma_{yy} + \sigma_{zz}}{3} \tag{2.14}$$

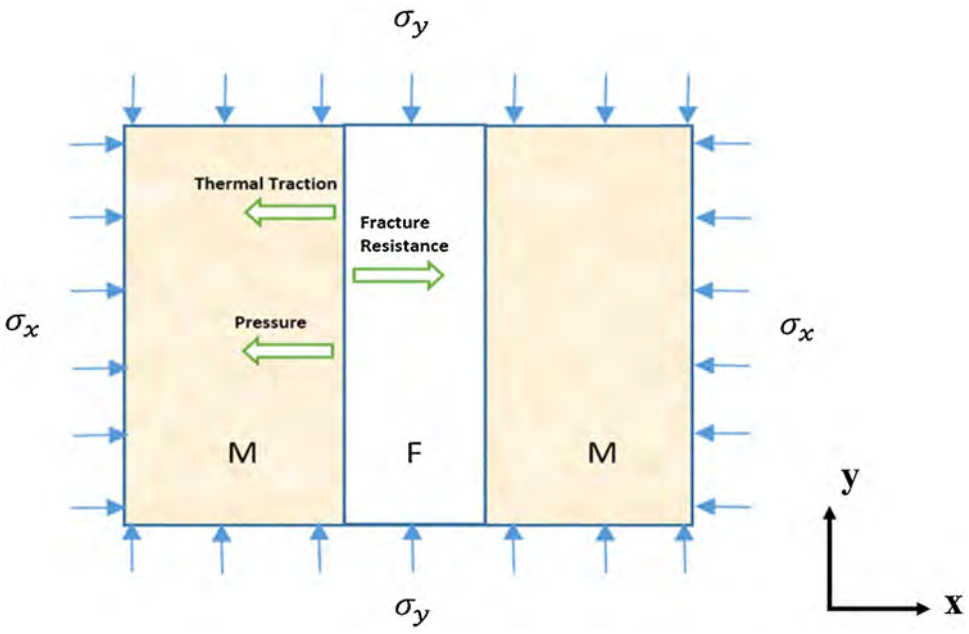

Fig. 3. Conceptual model of fracture resistance.

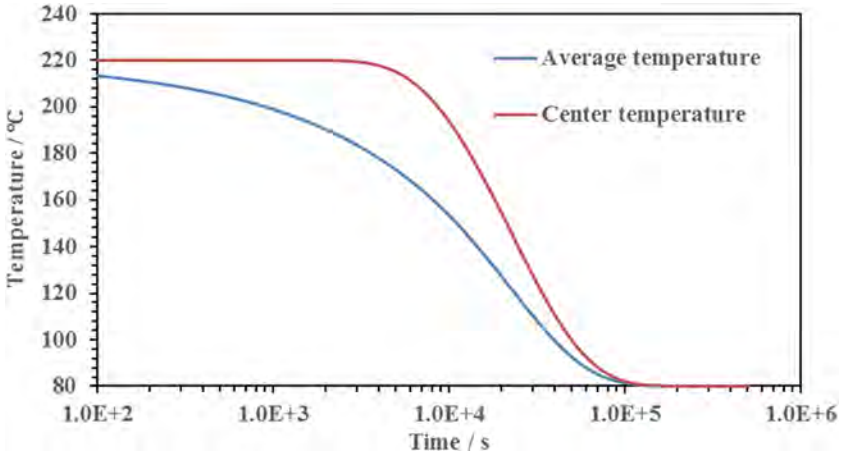

Fig. 4. Comparison between average matrix temperature and the temperature at the center of the matrix rock.

is the mean stress.

Recall the thermo-poro-elastic version of Navier's equation (Eslami et al., 2013)

$$\alpha\nabla P + 3\beta_T K\nabla T + (\lambda + G)\nabla\left(\nabla\times\vec{u}\right) + G\nabla^2\vec{u} + \vec{F} = 0 \tag{2.15}$$

The above Navier's equation has the displacement vector and cross partial derivatives, making it difficult to be solved. We implement divergence to the above equation

$$\alpha\nabla^2 P + 3\beta_T K\nabla^2 T + (\lambda + 2G)\nabla^2(\nabla\cdot\rightarrow u) + \nabla\cdot\rightarrow F = 0 \tag{2.16}$$

in which the divergence of the displacement can be conveniently expressed as the volumetric strain.

$$\nabla\times\rightarrow u = \varepsilon_v \tag{2.17}$$

From Eq. (2.13), the volumetric strain can be expressed by mean stress σ_m. By substituting the expression of volumetric strain into Eq. (2.16) and rearranging it, we can get the following equation

$$\frac{3(1-\nu)}{(1+\nu)}\nabla^2\sigma_m + \nabla\times\vec{F} = \frac{2(1-2\nu)}{(1+\nu)}\left(\alpha\nabla^2 P + 3\beta_T K\nabla^2 T\right) \tag{2.18}$$

The above equation is the governing equation of mechanical simulation for single-continuum.

Here each continuum has its unique pore pressure and temperature, meanwhile all continua share the same stress and strain. The relationship among the modulus is as follows.

$$E = 2G(1+\nu) = 3K(1-2\nu) \tag{2.19}$$

$$\lambda = \frac{2\nu G}{1-2\nu} \tag{2.20}$$

The changes in the porosity of the matrix rock by changes in pore pressure and temperature are calculated as (Rutqvist et al., 2002),

$$\phi = \phi_r + (\phi_0 - \phi_r)\exp\left(-a\times\sigma_m'\right) \tag{2.21}$$

In the above equation, ϕ_0 is the porosity at zero effective stress and ϕ_r is the residual porosity at high effective stress. a is an parameter determined by experiments.

Alternatively, the porosity could be also calculated via the following correlation.

$$\phi = \phi_0\left[1 + c_p\left(P - P_{ref}\right) + 3\beta_T\left(T - T_{ref}\right)\right] \tag{2.22}$$

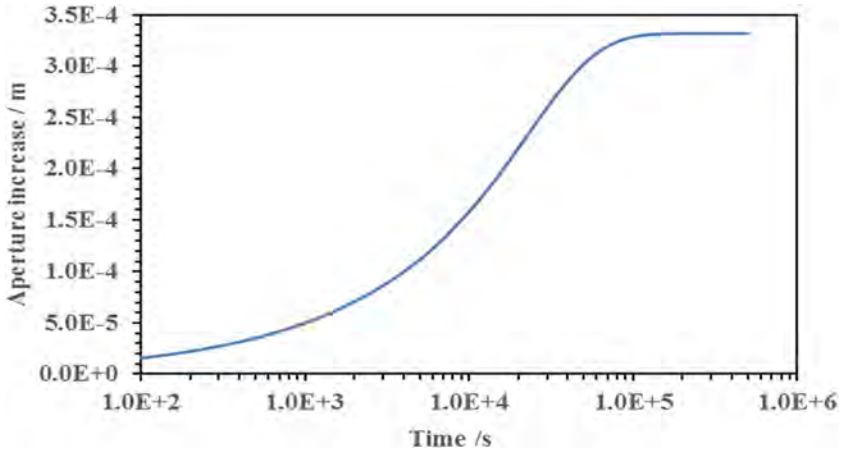

Fig. 5. Fracture aperture change versus time.

where c_p is the pore compressibility and β_T is the thermal expansion coefficient. P_{ref} and T_{ref} is the reference pressure and reference temperature respectively.

Changes in matrix permeability are calculated, based on changes in the porosity, using Carman-Kozeny equation (Carman, 1956; Kozeny, 1927) as,

$$K_m = K_{m0}\left(\frac{1-\phi_0}{1-\phi}\right)^3\left(\frac{\phi}{\phi_0}\right)^3 \tag{2.23}$$

We use Integral Finite Difference (IFD) method to solve the governing equations, e.g. (Narasimhan and Witherspoon, 1976; Celia et al., 1990). Using the IFD method, the governing equations are discretized as the following general form

$$\frac{V^{i+1}M^{k,i+1} - V^iM^{k,i}}{\Delta t} = \sum_m A_{nm}F^k_{nm} + q^k \tag{2.24}$$

In the above equation, i denotes a certain time step, m denotes a certain connection between two neighboring blocks, and n denotes a certain weighting scheme. The above nonlinear equations are solved by the Newton-Raphson method. Basically, IFD calculates the mass/energy accumulation within its grid blocks and the flux term on the interface between two neighboring grid blocks. Then all the terms are summed up and substituted into the Jacobian matrix for nonlinear iteration.

4. Semi-analytical correlation of fracture aperture change

4.1. Derivation of the correlation

In this work, a semi-analytical fracture aperture correlation is developed. The method is essentially analogous to Warren and Root's way of calculating the shape factor of fractures (Warren and Root, 1963).

A conceptual model of the classical dual-porosity is shown in the left of Fig. 1. Firstly proposed by Warren and Root (1963), this model characterizes the matrix rock as a low permeable block embedded in a fracture network. The connection between the matrix block and the fracture is determined by the shape factor (Warren and Root, 1963). The average pressure of the matrix and the fracture is $\overline{P_m}$ and P_f respectively, while the average temperature of the matrix and the fracture is $\overline{T_m}$ and T_f respectively.

Consider a matrix block surrounded by fractures of length L_i on the ith direction. Analogous to the derivation of shape factor by Lim and Aziz (1995), the temperature and pressure in the fractures are kept constant, respectively P_f and T_f. The initial temperature and pressure of the matrix block is P_{m0} and T_{m0}.

If the matrix permeability is low enough, which is the case of hot dry rock (HDR) and certain unconventional resources, the fluid convection effect in the matrix is not comparable to the heat conduction effect. Therefore, the leak off effect can be neglected in many cases without a fundamental change on the final results.

We start our derivation with the case of three sets of fractures. We treat the 3-D matrix block as a spherical body surrounded by the fracture system. Such approximation is similar to Warren and Root's derivation of the shape factor (Warren and Root, 1963). Similar to that used in (Warren and Root, 1963), we introduce the concept of 'characteristic length' to estimate the fracture behavior. The matrix block can approximated as an equivalent sphere with radius to be the characteristic length L_C. Therefore, the consistency of the volume between the sphere and the matrix block leads to

$$\frac{4}{3}\pi L_C^3 = L_x \times L_y \times L_z \tag{3.1}$$

Then L_C can be solved as

$$L_C = 0.62\left(L_x \times L_y \times L_z\right)^{1/3} \tag{3.2}$$

Specially, if $L_x = L_y = L_z = L$
Then

$$L_C = 0.62L \tag{3.3}$$

In a radial coordinate, the governing displacement Eq. (2.15) inside the sphere can be reduced to 1-D, as

$$\frac{\partial}{\partial r}\left[\frac{1}{r^2}\frac{\partial}{\partial r}\left(r^2u_r\right)\right] = \frac{1+\nu}{1-\nu}\beta\frac{\partial}{\partial r}\left(T_m - T_{m0}\right) \tag{3.4}$$

with the boundary condition at the center of the matrix block (Eslami et al., 2013)

$$u_r\left(r=0,t\right) = 0 \tag{3.5}$$

In the above equation, the pressure increase effect inside the matrix block is ignored. This is because that, compared to the thermal process, the hydraulic process has much smaller impact on the deformation of the matrix rock, especially for granite-type rock with low porosity and high modulus. This can be seen in the field scale session of this paper.

The above equation can be solved with a general solution as

$$u_r = \frac{1+\nu}{1-\nu}\beta\frac{1}{r^2}\int_0^r\left(T_m - T_{m0}\right)r^2dr + Cr \tag{3.6}$$

in which C is a constant to be determined by the other boundary condition, which is the stress condition at the fracture-matrix interface.

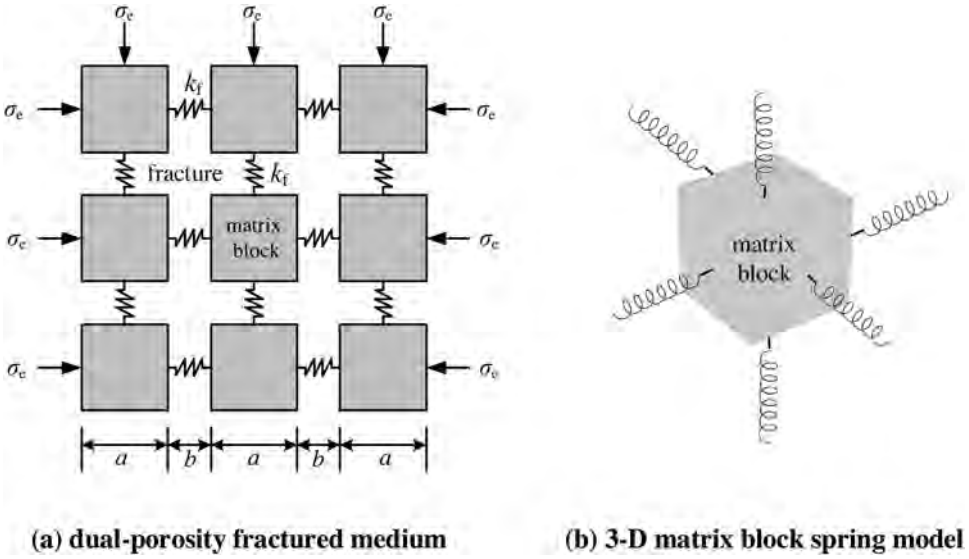

Fig. 6. Schematic of dual-porosity model and its spring model for a matrix block.

The change of normal stress inside the matrix block can be calculated from displacement, as shown in the following equation

$$\Delta\sigma_{rr} = \frac{E_m}{(1+\nu)(1-2\nu)} \left[(1-\nu)\frac{\partial u_r}{\partial r} + 2\nu\frac{u_r}{r} - (1+\nu)\beta\left(T_m - T_{m,0}\right)\right] \tag{3.7}$$

The boundary condition on the matrix-fracture interface is essentially a force balance condition, as shown in the following equation

$$\Delta\sigma_{rr}|_{r=L_C} = -k_f u|_{r=L_C} - \left(P_f - P_{f0}\right) \tag{3.8}$$

where P_f is the pressure in the fracture and k_f is the mechanical stiffness of the fracture Fig. 2. Here the fracture is treated as a linear spring and $-k_f u\left(L/2\right)$ is the resistance force of the fractured material. Note that the temperature and pressure gradient at the fracture-matrix interface is typically perpendicular to the fracture plane, therefore the above assumption is reasonable. If the fracture is treated as vacant, then k_f is zero. Note that since the displacement points inward, there should be a negative sign in front of the resistance force. The coceptual model of fracture resistance is shown in Fig. 3. Conceptual model of dual-porosity model. Left: matrix blocks and fracture system; Right: fluid flow inside the matrix-fracture system.

As to the integral, using the concept of dual continuum, we can get

$$\frac{1}{r^2}\int_0^{L_C}\left(T_m - T_{m0}\right)r^2 dr = \frac{1}{3}L_C\left(\bar{T}_m - T_{m0}\right) \tag{3.9}$$

By substituting the formulation of the normal stress at the matrix-fracture interface into the boundary condition, we can solve the constant C as

$$C = \frac{-\left(P_f - P_{f0}\right) + \frac{1}{3}\beta\left(\bar{T}_m - T_{m0}\right)\frac{2E_m}{1-2\nu} - \frac{1}{3}k_f\frac{1+\nu}{1-\nu}\left(\bar{T}_m - T_{m0}\right)L_C}{\frac{E_m}{1-2\nu} + k_f L_C} \tag{3.10}$$

Note that here k_f is treated as a constant value. It can also be a function of the displacement of fracture-matrix interface, as

$$k_f = k_f\left[u\left(L_c\right)\right] \tag{3.11}$$

Then C may cannot be expressed explicitly and should be solved iteratively.

Under the assumption of constant fracture stiffness, the displacement at matrix-fracture interface is

$$u_i = \frac{-\left(P_f - P_{f0}\right) + \beta\left(\bar{T}_m - T_{m0}\right)E_m'}{E_m' + k_f L_C} \times L_C \tag{3.12}$$

The fracture aperture change is two times the absolute value of fracture-matrix interface displacement

$$\Delta b_i = -2u_i\left(L_c\right) \tag{3.13}$$

Then the fracture aperture change can be expressed as

$$\Delta b_i = 2\frac{\left(P_f - P_{f0}\right) - \beta\left(\bar{T}_m - T_{m0}\right)E_m'}{E_m' + k_f L_C} \times L_C \tag{3.14}$$

In the cases with two sets of fractures, the matrix block is treated as a circle and the characteristic length is

$$L_C = 0.56\left(L_x \times L_y\right)^{1/2} \tag{3.15}$$

In the cases with one set of fractures, the characteristic length is simply

$$L_C = L_x \tag{3.16}$$

It can be easily proven that, using the concept of characteristic length, in the two-set fracture case and the one-set fracture case, the fracture aperture change have the same formulation as that in the three-set fracture case.

Based on the fracture aperture change correlation, the fracture permeability can be calculated by cubic law as

$$K_{fi} = C_i\frac{\left(b_{i0} + \Delta b_i\right)^3}{12L_i} \tag{3.17}$$

where C_i is a parameter to correlate between the mechanical aperture and the hydraulic aperture. Several preceding works (Witherspoon et al., 1979, 1980; Renshaw, 1995; Cappa et al., 2005) have investigated the relationship between the mechanical aperture b_m and the hydraulic aperture b_h. According to their work, when fracture apertures exceed 10 μm, the mechanical aperture and the hydraulic aperture are close to each other. In this work, all fracture aperture exceed 10 μm, therefore C_i is set to be 1.

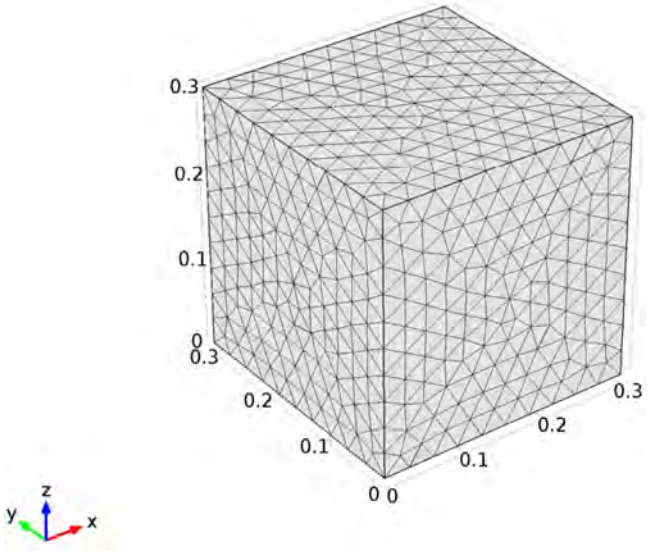

Fig. 7. FEM meshing for a matrix block simulation model.

Another option to calculate the transient fracture permeability is to correlate it with the initial fracture permeability as

$$K_{fi} = K_{fi0}\frac{(b_{i0} + \Delta b_i)^3}{(b_{i0})^3} \tag{3.18}$$

4.2. Numerical verification

We use analytical solutions to show the basic features of our newly proposed correlation. Also, we use commercial software, COMSOL Multiphysics, to do refined simulation to show the accuracy of this correlation.

In 1-D system, if the leak-off effect is ignored, the thermal governing equation in the matrix can be reduced to

$$(1-\phi)K\nabla^2 T_m = (1-\phi)\rho_R C_R\frac{\partial T_m}{\partial t} \tag{3.19}$$

By implementing the boundary and initial conditions

$$T_m(x=0,t) = T_f \tag{3.20}$$

$$T_m(0 < x < L_i, t=0) = T_0 \tag{3.21}$$

The governing equation can be solved as

$$T_m = T_f + \sum_{n=1}^{\infty}\frac{4\left(T_{ini}-T_f\right)}{(2n-1)\pi}\sin\left[\frac{(2n-1)\pi}{L_i}x\right]$$

$$\exp\left[-\frac{K}{\rho_R C_R}\frac{(2n-1)^2\pi^2}{L_i^2}t\right] \tag{3.22}$$

The matrix temperature at the center (x = L/2) is

$$T_m\left(\frac{L_i}{2}\right) = T_f + \sum_{n=1}^{\infty}\frac{4\left(T_{ini}-T_f\right)}{(2n-1)\pi}\sin\left[\frac{(2n-1)\pi}{2}\right]$$

$$\exp\left[-\frac{K}{\rho_R C_R}\frac{(2n-1)^2\pi^2}{L_i^2}t\right] \tag{3.23}$$

The average temperature of matrix rock $\overline{T_m}$ is

$$\overline{T_m} = \frac{\int_0^{L_i} T_m dx}{L_i} = T_f + \sum_{n=1}^{\infty}\frac{8\left(T_{ini}-T_f\right)}{(2n-1)^2\pi^2}$$

$$\exp\left[-\frac{K}{\rho_R C_R}\frac{(2n-1)^2\pi^2}{L_i^2}t\right] \tag{3.24}$$

We choose the following parameters

By substituting the above parameters into the formulations, we can calculate $T_m\left(L/2\right)$ and $\overline{T_m}$. The results are shown in Fig. 4.

The fracture aperture change is plotted Fig. 5. As we can see, the fracture aperture will rapidly increase within one hour.

We then use the commercial software COMSOL Multiphysics as a benchmark to verify our correlation. COMSOL Multiphysics is a powerful numerical tool for the simulation of multi-physical fields. It is based on the finite element method. The technical details of it can be found in (COMSOL, 2008) Fig. 5.

We use COMSOL Multiphysics to simulate the thermo-mechanical behavior of one matrix block that is surrounded by fractures. The matrix block is initially 220 °C, while the temperature of the surrounding fractures is kept as 80 °C. The other parameters are all shown in Table 1. The model and the generated mesh are shown in Figs. 6 and 7 respectively. In our simulation model, two physics modules are applied, i.e., the solid mechanics module and the heat transfer in solids module. The key point is the spring boundary conditions are applied to simulate the aperture change of the fracture in solid mechanics module.

Starting from time t = 0s, the cooling front starts to penetrate into the matrix, causing the matrix temperature to decrease, there-

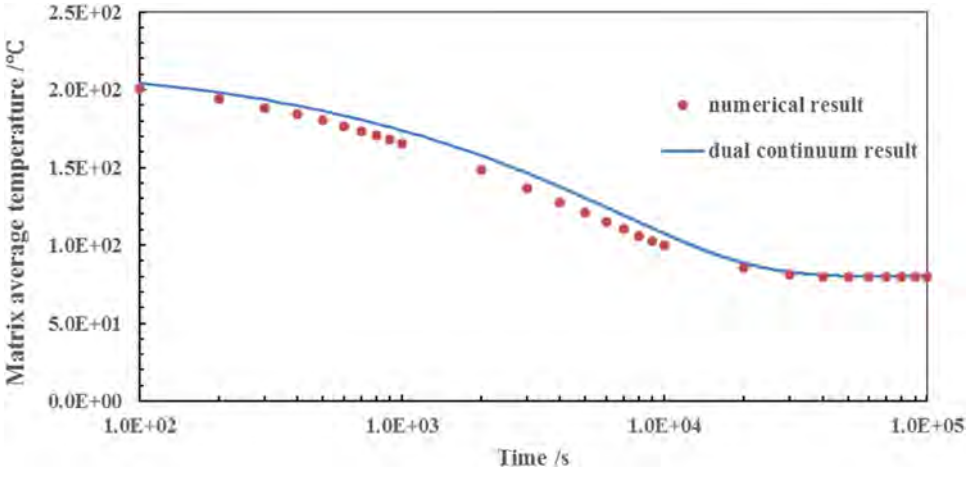

Fig. 8. comparison between the temperature profiles of the refined numerical simulation and the dual continuum approach.

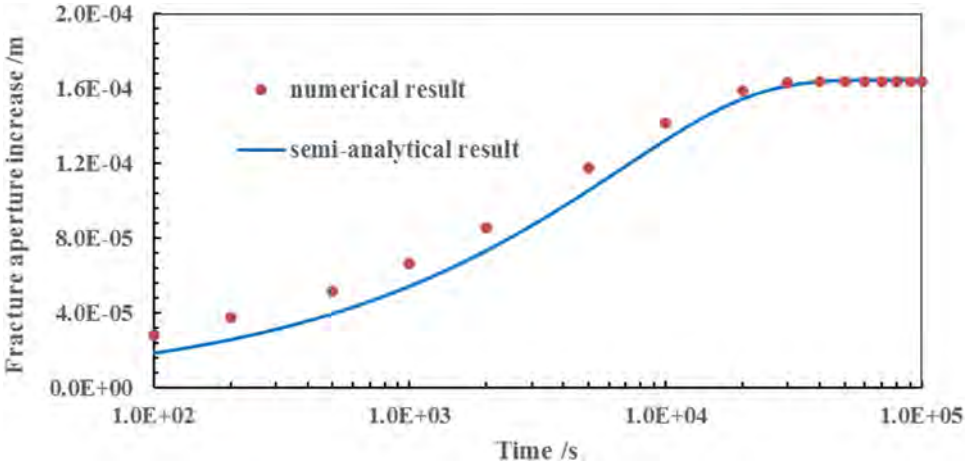

Fig. 9. the red dots indicate the results of the refined numerical simulation, while the blue line indicates our semi-analytical results based on dual continuum approach (For interpretation of the references to colour in this figure legend, the reader is referred to the web version of this article.).

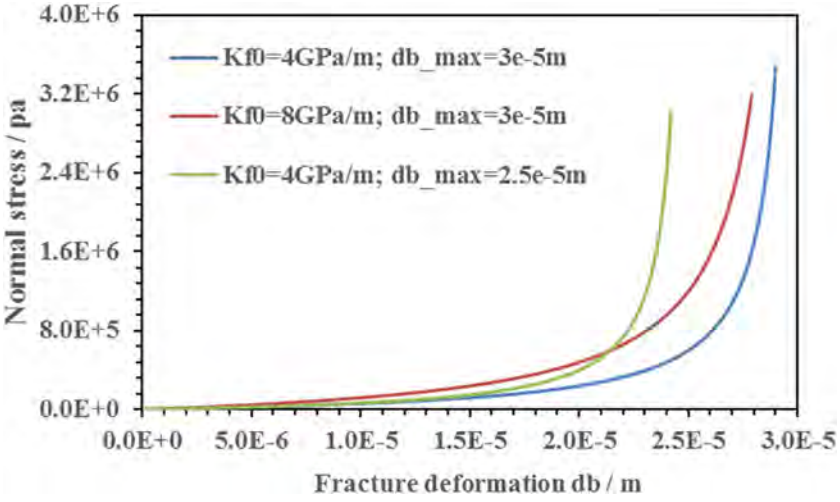

Fig. 10. typical normal stress-normal closure curve of Barton-Bandis' correlation (Hsiung et al., 2005).

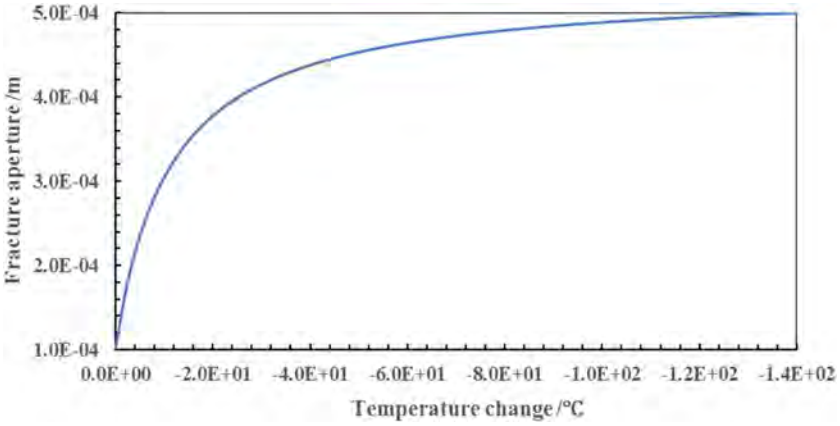

Fig. 11. Temperature decrease (thermal unloading process) combined Barton-Bandis' correlation.

fore the matrix formation to shrink. We record the transient matrix average temperature and the fracture aperture values with respect to time. We compare the results provided by this refined simulation with the results predicted by our semi-analytical approach, in which we use the dual porosity model to calculate matrix average temperature and use the proposed correlation to calculate the fracture aperture. The results are shown in Figs. 8 and 9. From Fig. 8, we can see that the average temperature obtained from the refined simulation is very close to the result of dual continuum method. The difference between them is about 5% to 9%. Meanwhile, from Fig. 9, we can see that our semi-analytical approach predicts reasonable fracture aperture results, compared to the refined numerical sim-

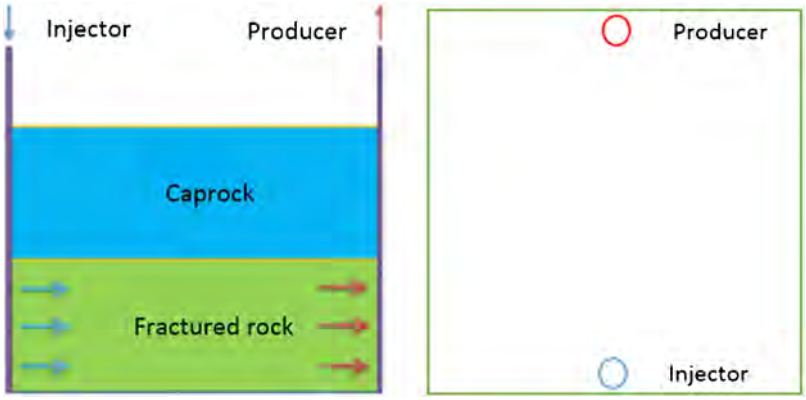

Fig. 12. Left: conceptual model of water cycling system; right: bird-view of the problem showing the location of the injector and the producer.

Table 1
Input parameters for calculating matrix temperature and aperture change.

Properties	Values	Units
Young's modulus	66.0	GPa
Fracture spacing	0.3	m
Poisson's ratio	0.25	dimensionless
Biot's coefficient	1.0	dimensionless
Linear thermal expansion coefficient	7.9	10^{-6} m/(m K)
Thermal conductivity of dry rock	1.0	W/(m K)
Heat capacity of rock	1000	J/(kg K)
Initial temperature of matrix	220	°C
Fracture temperature	80	°C
Density of rock	2.5	10^3 kg/m3

ulation. While at the beginning the relative error is about 14%, the relative error quickly decreases. Our results match very well with numerical simulation at the late stage of the problem. We should note that, the temperature used in our semi-analytical approach is from dual continuum method, therefore, as long as our semi-analytical approach has the same level of accuracy as the dual continuum method, our proposed approach shall be judged as enough accurate in real practice.

5. Coupling with Barton-Bandis' correlation

As mentioned in the previous sessions, our approach can also be coupled with existing fracture normal closure correlations, such as the Barton-Bandis' correlation. When coupled with the either the hyperbolic model or the logarithmic model, the fracture stiffness cannot be treated as a constant anymore. Instead, it should be treated as a function of the normal effective stress. In this paper, we use (Hsiung et al., 2005)'s approach to couple our formulation with Barton-Bandis' correlation.

We rewrite the Barton-Bandis' correlation as

$$\Delta b = \frac{M\sigma_n^{'}}{N\sigma_n^{'}+1} \tag{4.1}$$

$$\sigma_n^{'} = \frac{\Delta b}{M - N\Delta b} \tag{4.2}$$

where Δb is the fracture aperture change. M and N are predetermined parameters by laboratory.

Based on Eq. (3.13), the fracture aperture change can be correlated with the fracture-matrix interface displacement as

$$\Delta b = -2u(L_C) \tag{4.3}$$

Therefore, the fracture aperture can be calculated by

$$b = b_0 + \Delta b = b_0 - 2u(L_C) \tag{4.4}$$

where b_0 is the initial fracture aperture.

According to (Hsiung et al., 2005), M can be calculated approximately as

$$M = \frac{1}{K_{f0}} \tag{4.5}$$

where K_{f0} is the initial stiffness of the fracture.

N can be calculated approximately as

$$N = \frac{-1 + \sqrt{1 + 4\sigma_n^{'} M b_r^{-1}}}{2\sigma_n^{'}} \tag{4.6}$$

where $\sigma_{nr}^{'}$ is a reference effective normal stress and b_r is a reference fracture aperture. The maximum fracture aperture is

$$\Delta b_{\max} = \frac{M}{N} \tag{4.7}$$

The details of this derivation can be found in (Hsiung et al., 2005). The typical curves predicted by Barton-Bandis model with respect to different combination of initial fracture stiffness and maximum fracture aperture are plotted in Fig. 10.

With the above formulation, the boundary condition at the fracture-matrix interface should be

$$-f[u] - \Delta P_f = -\frac{[b_{\max} - (b_0 - 2u(a))]}{M - N[b_{\max} - (b_0 - 2u(a))]} + (\sigma_{n0} - P_0) + \left(P_0 - P_f\right) \tag{4.8}$$

where σ_{n0} is the initial in-situ normal stress of the reservoir and b_0 is the initial fracture aperture. By implementing this boundary condition, the constant C as well as fracture aperture change can be solved either analytically or numerically. If the fracture normal closure is too complex to get an explicitly expression of the constant C, the equation can be solved by nonlinear iterative methods with very simple computer program.

Given $b_{\max} = 5e-4m, K_{fn0} = 2\text{GPa/m}$ and $b_0 = 1e-4\text{m}$ and using the parameters provided in Table 1, the fracture aperture with respect to temperature decrease is calculated, and shown in Fig. 11. Such result is qualitatively consistent with that in (Hsiung et al., 2005).

6. Numerical results

In the session, we apply our newly derived correlation to field scale problems. We aim to explain the significant increase of injectivity of cold water injectors in geothermal reservoirs. We use some parameters obtained from Habanero field, Cooper Basin, Australia. The reservoir mostly consists of granite. One cold water injector and one hot fluids producer locate symmetrically in the two boundaries of the fractured EGS reservoir. The fluids produced are rejected into the reservoir via the cold water injector. Meanwhile, the engineered

Table 2
Input parameters for hydraulic connected well pair case.

Properties	Values	Units
Initial permeability of the fracture continuum	$K_f = 1.0 \times 10^{-11}$	m^2
Initial permeability of the matrix continuum	$K_{mx} = 1.0 \times 10^{-15}$	m^2
Porosity of the matrix at zero stress	0.04	dimensionless
Residual porosity of the matrix	0.01	dimensionless
Parameter *a* for porosity	1e-8	dimensionless
Initial porosity of the fracture	0.001	dimensionless
Young's modulus	66.0	GPa
Fracture spacing	0.3	m
Poisson's ratio	0.25	dimensionless
Biot's coefficient	0.7	dimensionless
Linear thermal expansion coefficient	7.9	10^{-6} m/(m K)
Thermal conductivity of dry rock	1.0	W/(m K)
Heat capacity of rock	1000	J/(kg K)
Density of rock	2.5	10^3 kg/m3
Vertical stress	90	MPa
Maximum horizontal stress	140	MPa
Minimum horizontal stress	110	MPa
Fracture stiffness	4	GPa/m

fractures inside the reservoir hydraulically connect the two wells, creating a cycling system.

Chen and Wyborn (2009) have briefly studied this problem using discrete fracture approach with Excel. In their work, they assumed the fluid flow to be isothermal and ignored the mechanical effect. However, as illustrated in the previous sections, thermal and mechanical processes are rather important in geothermal problems and cannot be simply ignored.

In our work, the EGS reservoir is simulated with the dual-porosity approach. The problem in interest is of 2500 ft × 2500 ft × 500 ft (762 m × 762 m × 152 m). The initial pressure is 7.0 MPa and the initial temperature is 220 °C.

The problem description is shown in Fig. 12.

A case has been run, of which the input parameters are listed in Table 2. As shown in Fig. 12, there should be an impermeable caprock zone above the geothermal layer. The vertical stress σ_v generated by the caprock is 90 MPa. The minimum horizontal stress is 110 MPa, while the maximum horizontal stress is 140 MPa (Chen and Wyborn, 2009).

The horizontal boundary condition of this problem is set to be uniaxial strain boundary, meaning that the horizontal boundaries are fixed with zero normal displacement. In this case, we directly give the in-situ mean stress on the boundary and run a 'symmetrical' problem on each boundary in order to force the normal displacement to be zero. Compaction force (vertical stress) is applied along the vertical direction, as shown by the upper part of Fig. 13. There is one set of along the horizontal direction, as shown by the lower part of Fig. 13.

Cold water of 80 °C is injected for 7 years at the constant rate of 12 kg/s from the injection well. The production well is producing at a constant bottomhole pressure (BHP) of 5.0 Mpa. The reservoir is 4 km in depth.

The change of the permeability field is shown in Fig. 14, from which we can see that the permeability has been enhanced by around 2 orders of magnitude. Such results are consistent with the observation from real reservoir production.

The initial aperture of fracture can be back calculated from the initial fracture permeability using the cubic law in Eq. (3.17). In this case, the initial fracture aperture is 330 μm along the horizontal direction.

The simulation is run on a PC with 8 processes involved. The results are as follows. The permeability fields after 180 days and 7 years of injection are plotted in Fig. 14. As shown by the figure, because of the high flux channel created by the hydraulic connected wells, the permeability enhancement has a front, demonstrating the major flow direction. The fracture pressure and temperature

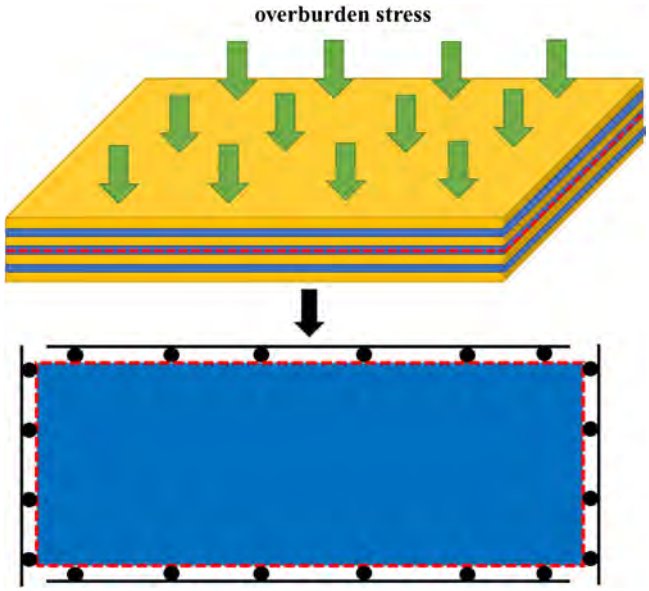

Fig. 13. conceptual model of the fractured geothermal reservoir with uniaxial strain boundary condition.

of injector is plotted in Fig. 15, and the fracture aperture and the fracture permeability is plotted in Fig. 16. The initial porosity of the matrix rock is calculated via Eq. (2.21) based on the given properties of the rock and the in-situ stress condition. The mass diffusion process is ignored in this study and only convection is considered.

As demonstrated by the results, while the fracture aperture is enhanced by 100%, the fracture permeability is enhanced much more greatly (800%) near the cold water injector. This is because of the cubic law, that the fracture permeability is very sensitive to fracture aperture.

Our results in Fig. 16 can be used to explain the increase of injectivity of certain reinjection wells (Sarmiento, 1986). As shown in Fig. 17, the injectivity of well 4R1 in the Tongonan field was significantly increased after the cold waster water reinjection. (The later reduction of the injectivity was attributed to the scaling near the well caused by injected debris.) The increase of well injectivity is of the same magnitude that is predicted by our model.

The sensitivity analysis of the fracture permeability at the injector with respect to injection temperature is shown in Fig. 18. As demonstrated by Fig. 18, if the injection temperature decreases from 80 °C to 70 °C, the eventual fracture permeability will increase

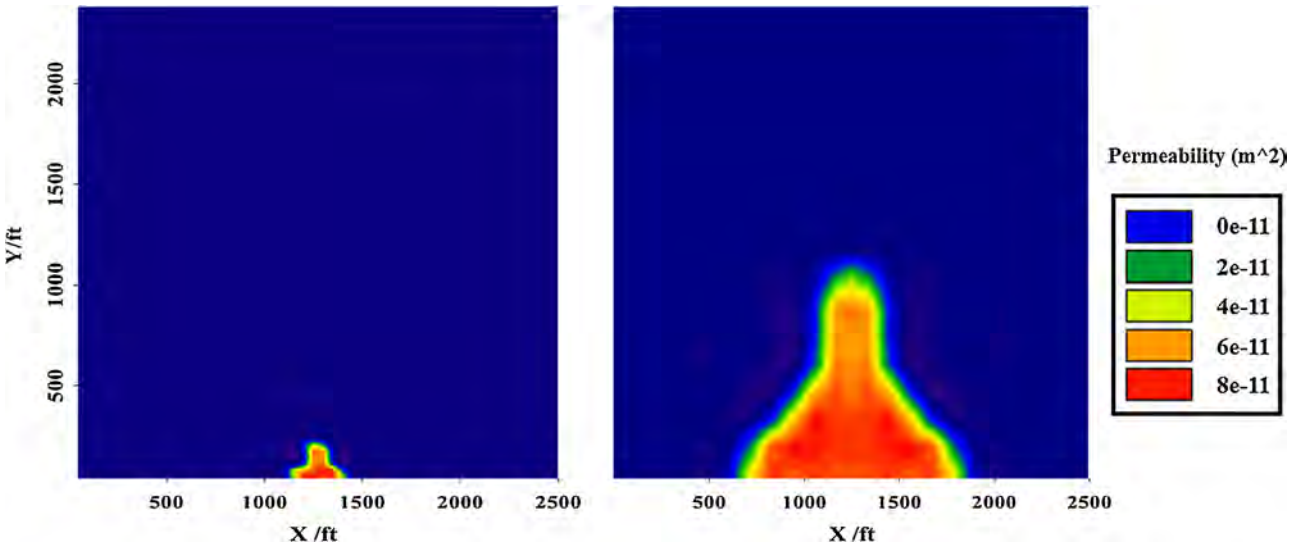

Fig. 14. Permeability change after cold water injection. Red/orange color indicates the permeability enhanced zone near the injector. The figure on the left is the y-permeability field at 180 days of injection, while the figure on the right is the y-permeability field at 7 years of injection. In this case $K_{f0} = 10^{-11}$ m^2 (~10 Darcy).

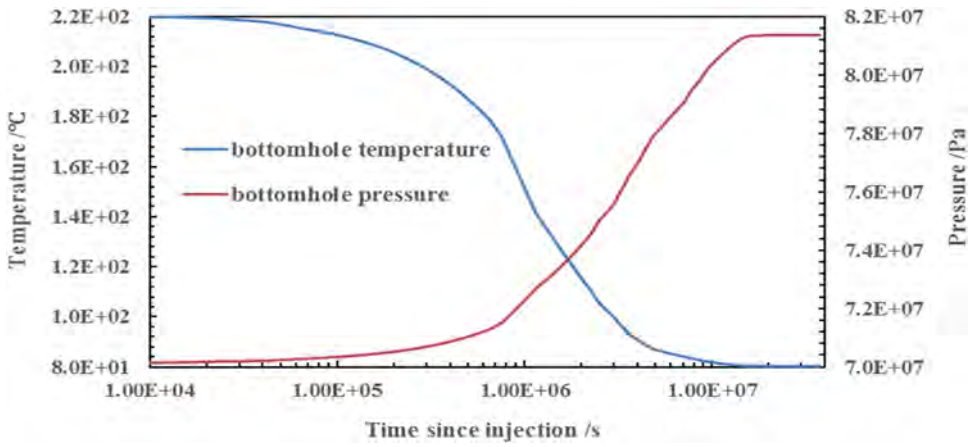

Fig. 15. Pressure and temperature curve at the cold water injector.

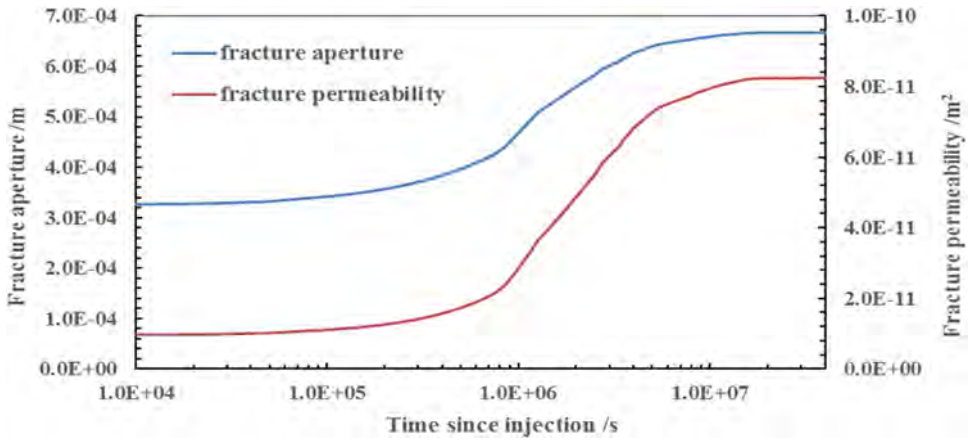

Fig. 16. Fracture aperture and fracture permeability at the cold water injector.

significantly from 8.22×10^{-11} m^2 to 9.12×10^{-11} m^2. And if the injection temperature increases from 80 °C to 90 °C, the eventual fracture permeability will decrease from 8.22×10^{-11} m^2 to 7.41×10^{-11} m^2.

The matrix permeability at the cold water injector with respect to the same change of injection temperature is shown in Fig. 19. Compared to the fracture permeability, it is obvious that the matrix is much less sensitive to temperature change. As such, the frac-

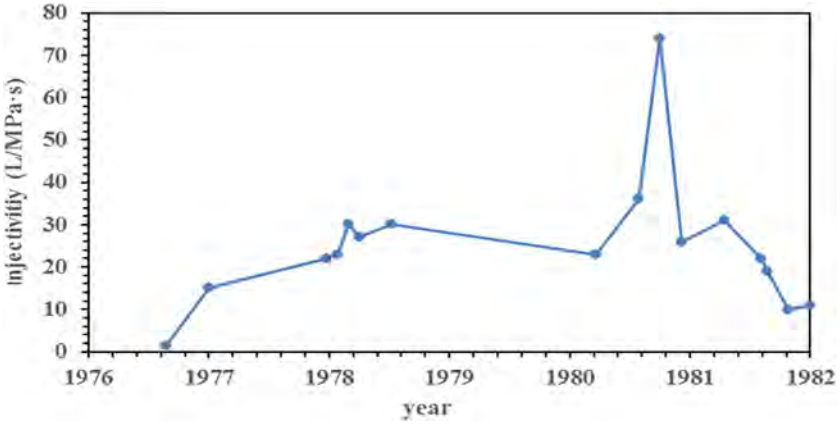

Fig. 17. Injectivity history of well 4R1 in the Tongonan field, Philippines. After (Sarmiento, 1986).

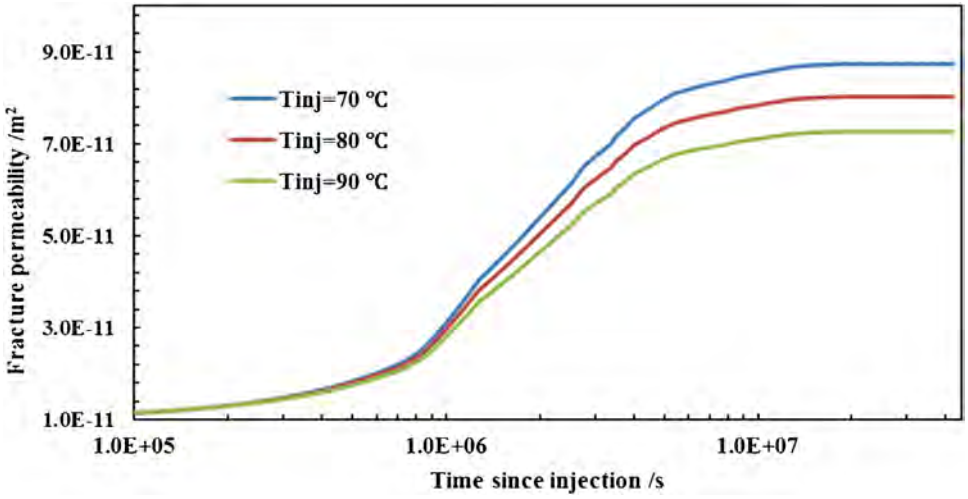

Fig. 18. Fracture permeability change at the cold water injector with different injection temperature and constant injection rate.

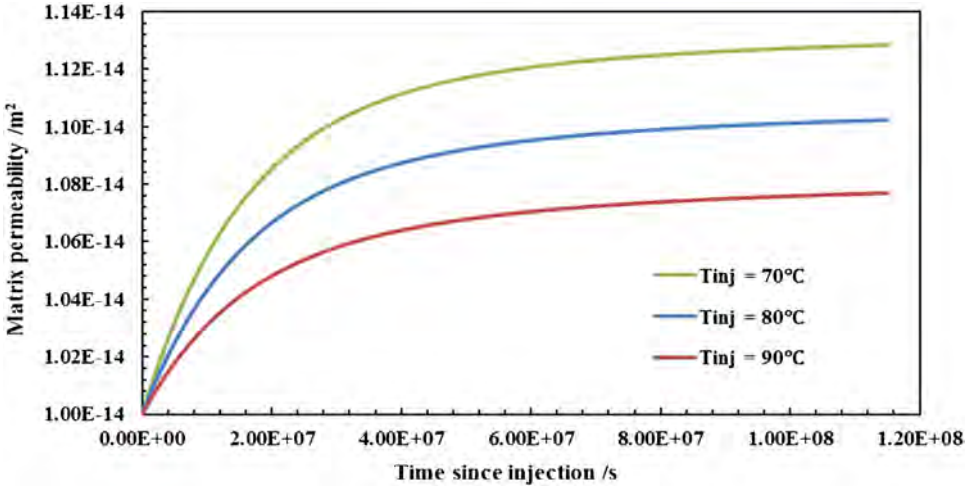

Fig. 19. matrix permeability at the cold water injector with different injection temperature.

ture is the key to understand the behavior of fractured geothermal reservoir.

Besides the injection temperature, the fracture permeability is also very sensitive to the thermal expansion coefficient β of the matrix rock, as shown in Fig. 20. This is because that thermal expansion coefficient is multiplied to the temperature change, therefore if the pressure increase is small, the fracture aperture change is close to linear relationship with the thermal expansion coefficient of the matrix rock.

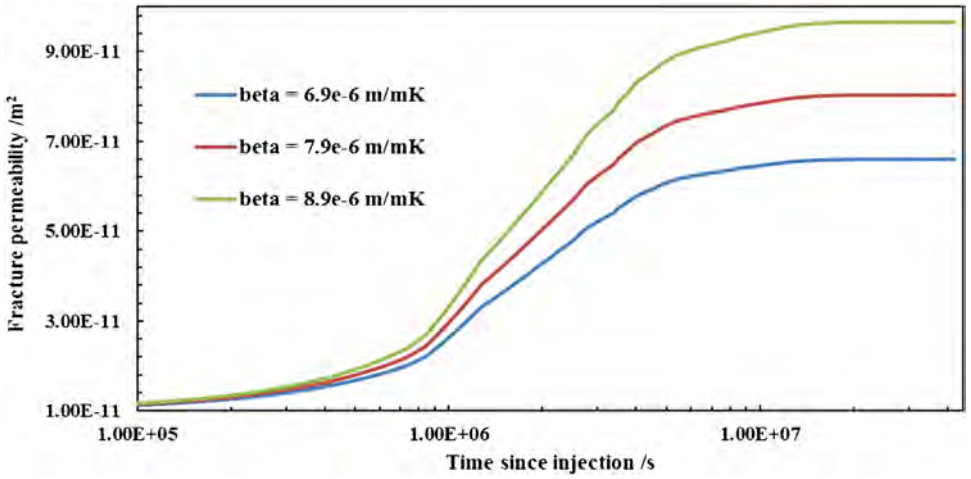

Fig. 20. Fracture aperture change versus time with different thermal expansion coefficients.

7. Discussion

In the above sessions, we have shown the basic features of our newly derived correlation. The advantage of our correlation is that it is based on semi-analytical derivation and it can be readily implemented in simulators with dual-porosity model. The correlation potentially has a wide range of application, since it does not have stress as input parameter and can be used in simulators without mechanical simulation module. However, our correlation may not as accurate as existing correlations which uses all the three components of the in-situ stress (Rutqvist et al., 2002; Rutqvist, 2008). Especially, our correlation cannot be applied in certain cases where uniaxial strain assumption is not valid

In this paper, we have shown the significant effect of thermal stress on the injectivity of the cold water injector.

With 10 °C decrease of injection temperature, the fracture permeability will be enhanced by 0.7–0.9 Darcy. The stiffer the rock is, the more sensitivity the fracture becomes. As shown in Fig. 15, while the temperature at the injection decreases by about 63%, the pressure only increases by 17%. In this way, the thermal effect on the fracture permeability is much larger than the hydraulic effect. Moreover, according to Eq. (3.14), the thermal effect is proportional to the Young's modulus of the matrix rock. As many geothermal reservoirs consists of granite with high Young's modulus, the thermal effect is even more significant than the hydraulic effect in this sense. Such truth also support our ignorance of the pore pressure increases in the derivation of the correlation, as the mechanical effect induced by the increase of pore pressure is much smaller than that induced by the temperature reduction.

8. Conclusion

In this work, we have developed a semi-analytical correlation to capture the fracture aperture/permeability change induced by cold water injection. Compared to the existing correlations, the newly proposed correlation is more practical and can reflect more physical process within the process of thermal induced fracture permeability alteration. The proposed correlation is able to quantify the effect of the hydraulic and thermal process respectively. Also, it can be coupled with existing mechanical correlations, e.g. Barton-Bandis correlation, to provide better prediction on the normal closure behaviors of fractures.

The new correlation has been implemented into our parallel simulator THM-EGS. We have used this proposed correlation to study a cold water injection problem of a hydraulic connected well pair. The results show that the fracture permeability can be enhanced by 700% by cold water injection. We also show that, compared with the matrix block, the fracture permeability is much more sensitive to the injection temperature as well as the thermal expansion coefficient of the matrix.

We can draw the conclusion that, temperature effects are very important in the recovery of geothermal energy and our proposed approach is able to capture the THM behaviors of fractured EGS reservoirs. With minor modification, the proposed correlation can also be applied to oil/gas reservoirs.

Acknowledgements

This work was supported by the National Natural Science Foundation of China (Grants 51404292 and 51234007), Shandong Provincial Natural Science Foundation, China (Grant ZR2014EEQ010), the Fundamental Research Funds for the Central Universities, China (15CX05037A, 14CX05027A). The authors would like to extend thanks to Energy Modeling Group (EMG) of Petroleum Engineering Department at Colorado School of Mines and Foundation CMG for the support of this research.

References

Alm, P., 1999. Hydro-Mechanical Behaviour of a Pressurised Single Fracture: An In-situ Experiment. Chalmers University of Technology.

Baghbanan, A., Jing, L., 2007. Hydraulic properties of fractured rock masses with correlated fracture length and aperture. Int. J. Rock Mech. Min. Sci. 44 (5), 704–719, http://dx.doi.org/10.1016/j.ijrmms.2006.11.001.

Bandis, S.C., Lumsden, A.C., Barton, N.R., 1983. Fundamentals of rock joint deformation. Int. J. Rock Mech. Min. Sci. Geomech. Abstr. 20 (6), 249–268, http://dx.doi.org/10.1016/0148-9062(83)90595-8.

Bandis, S., 1990. Mechanical properties of rock joints. Rock Joints. Balkema, Rotterdam. Retrieved from https://books.google.com/books?hl=en&lr=&id=00fDaqhru2cC&oi=fnd&pg=PA125dq=Mechanical+properties+of+rock+joints&ots=0PbKLxIByK&sig=WYEbgJP-KJoP_aMx9v8QGkxNvxM.

Barenblatt, G., Zheltov, I., Kochina, I., 1960. Basic concepts in the theory of seepage of homogeneous liquids in fissured rocks [strata]. J. Appl. Math. Mech. 24 (5), 1286–1303, http://dx.doi.org/10.1016/0021-8928(60)90107-6.

Barton, N., Bandis, S., Bakhtar, K., 1985. Strength, deformation and conductivity coupling of rock joints. Int. J. Rock Mech. Min. Sci. Geomech. Abstr. 22 (3), 121–140, http://dx.doi.org/10.1016/0148-9062(85)93227-9.

Berkowitz, B., 1995. Analysis of fracture network connectivity using percolation theory. Math. Geol. 27 (4).

Berkowitz, B., 2002. Characterizing flow and transport in fractured geological media: a review. Adv. Water Resour. 25 (8), 861–884, http://dx.doi.org/10.1016/S0309-1708(02)00042-8.

COMSOL., 2008. Multiphysics, C. O. M. S. O. L. 3.5 A User's Guide.

Cappa, F., Guglielmi, Y., Fénart, P., Merrien-Soukatchoff, V., Thoraval, A., 2005. Hydromechanical interactions in a fractured carbonate reservoir inferred from

hydraulic and mechanical measurements. Int. J. Rock Mech. Min. Sci. 42 (2), 287–306, http://dx.doi.org/10.1016/j.ijrmms.2004.11.006.
Carman, P.C., 1956. Flow of Gases Through Porous Media. Academic press.
Celia, M.A., Bouloutas, E.T., Zarba, R.L., 1990. A general mass-conservative numerical solution for the unsaturated flow equation. Water Resour. Res. 26 (7), 1483–1496, http://dx.doi.org/10.1029/WR026i007p01483.
Chang, M., 1993. Deriving the Shape Factor of a Fractured Rock Matrix (Retrieved from) http://www.osti.gov/scitech/biblio/10192737.
Chen, D., Wyborn, D., 2009. Habanero field tests in the cooper basin, Australia : a proof-of-concept for EGS. GRC Trans., 33.
Eslami, M., Hetnarski, R., Ignaczak, J., Noda, N., Sumi, N., 2013. Theory of Elasticity and Thermal Stresses. Springer, New York (Retrieved from) http://link.springer.com/content/pdf/10.1007/978-94-007-6356-2.pdf.
Evans, K.F., Cornet, F.H., Hashida, T., Hayashi, K., Ito, T., Matsuki, K., Wallroth, T., 1999. Stress and rock mechanics issues of relevance to HDR/HWR engineered geothermal systems: review of developments during the past 15 years. Geothermics 28 (4), 455–474, http://dx.doi.org/10.1016/S0375-6505(99)00023-1.
Fakcharoenphol, P., Hu, L., Wu, Y.-S., 2012. Fully-implicit flow and geomechanics model: application for enhanced geothermal reservoir simulations. Proceedings of the 37th Workshop on Geothermal Reservoir Engineering.
Fung, L.S.K., Buchanan, L., Wan, R.G., 1994. Coupled geomechanical-thermal simulation for deforming heavy-oil reservoirs. J. Can. Pet. Technol. 33 (04), http://dx.doi.org/10.2118/94-04-03.
Gelet, R., Loret, B., Khalili, N., 2012. A thermo-hydro-mechanical coupled model in local thermal non-equilibrium for fractured HDR reservoir with double porosity. J. Geophys. Res.: Solid Earth 117 (B7), http://dx.doi.org/10.1029/2012jb009161, n/a–n/a.
Ghassemi, A., Suresh Kumar, G., 2007. Changes in fracture aperture and fluid pressure due to thermal stress and silica dissolution/precipitation induced by heat extraction from subsurface rocks. Geothermics 36 (2), 115–140, http://dx.doi.org/10.1016/j.geothermics.2006.10.001.
Gilman, J.R., Kazemi, H., 1983. Improvements in simulation of naturally fractured reservoirs. Soc. Pet. Eng. J. 23 (04), 695–707, http://dx.doi.org/10.2118/10511-PA.
Hsiung, S.M., Chowdhury, A.H., Nataraja, M.S., 2005. Numerical simulation of thermal—mechanical processes observed at the drift-scale heater test at yucca mountain, nevada, USA. Int. J. Rock Mech. Min. Sci. 42 (5), 652–666, http://dx.doi.org/10.1016/j.ijrmms.2005.03.006.
Hu, L., Winterfeld, P.H., Fakcharoenphol, P., Wu, Y.-S., 2013. A novel fully-coupled flow and geomechanics model in enhanced geothermal reservoirs. J. Pet. Sci. Eng. 107, 1–11, http://dx.doi.org/10.1016/j.petrol.2013.04.005.
Itasca, Consulting Group Inc., 1997. FLAC3D Manual: fast Lagrangian analysis of continua in 3 dimensions—version 2.0. Minnepolis.
Jaeger, J., Cook, N., Zimmerman, R., 2009. Fundamentals of Rock Mechanics (Retrieved from) https://books.google.com/books?hl=en&lr=&id=PbMqM8GH9-IC&oi=fnd&pg=PR9&ots=PYHCl_-Axz&sig=nRQOsiY51gwhJM5GVmSMwfgsi7M.
Kaya, E., Zarrouk, S.J., O'sullivan, M.J., 2011. Reinjection in geothermal fields: a review of worldwide experience. Renew. Sustain. Energy Rev. 15 (1), 47–68, http://dx.doi.org/10.1016/j.rser.2010.07.032.
Kazemi, H., Merrill, L.S., Porterfield, K.L., Zeman, P.R., 1976. Numerical simulation of water-oil flow in naturally fractured reservoirs. Soc. Pet. Eng. J. 16 (06), 317–326, http://dx.doi.org/10.2118/5719-PA.
Kim, J., Sonnenthal, E.L., Rutqvist, J., 2012. Formulation and sequential numerical algorithms of coupled fluid/heat flow and geomechanics for multiple porosity materials. Int. J. Numer. Methods Eng. 92 (5), 425–456, http://dx.doi.org/10.1002/nme.4340.
Kozeny, J., 1927. Über Kapillare Leitung Des Wassers Im Boden:(Aufstieg: Versickerung Und Anwendung Auf Die Bewässerung). Hölder-Pichler-Tempsky.
Lim, K.T., Aziz, K., 1995. Matrix-fracture transfer shape factors for dual-porosity simulators. J. Petrol. Sci. Eng. 13 (3), 169–178, http://dx.doi.org/10.1016/0920-4105(95)00010-F.
Lu, H., Di Donato, G., Blunt, M.J., 2008. General transfer functions for multiphase flow in fractured reservoirs. SPE J. 13 (03), 289–297, http://dx.doi.org/10.2118/102542-PA.
Majer, E., Peterson, J., 2007. The impact of injection on seismicity at the geysers, california geothermal field. Int. J. Rock Mech. (Retrieved from) http://www.sciencedirect.com/science/article/pii/S1365160907001207.
McTigue, D.F., 1986. Thermoelastic response of fluid-saturated porous rock. J. Geophys. Res. 91 (B9), 9533, http://dx.doi.org/10.1029/jb091ib09p09533.
Moinfar, A., Narr, W., Hui, M.-H., Mallison, B.T., Lee, S.H., 2011. Comparison of discrete-fracture and dual-permeability models for multiphase flow in naturally fractured reservoirs. In: SPE Reservoir Simulation Symposium. Society of Petroleum Engineers, http://dx.doi.org/10.2118/142295-ms.
Narasimhan, T.N., Witherspoon, P.A., 1976. An integrated finite difference method for analyzing fluid flow in porous media. Water Resour. Res. 12 (1), 57–64, http://dx.doi.org/10.1029/WR012i001p00057.
Norris, A., 1992. On the correspondence between poroelasticity and thermoelasticity. J. Appl. Phys. 71 (3), 1138, http://dx.doi.org/10.1063/1.351278.
Nowacki, W., 2013. Thermoelasticity, 2nd ed. Pergamon Press Inc., Elmsford, New York, Retrieved from https://books.google.com/books?hl=en&lr=&id=muEgBQAAQBAJ&oi=fnd&pg=PP1&dq=Thermoelasticity&ots=hFzxn9XXKx&sig=ol3vL5u2-rKdlULhCPaPb-F3DSI.
Pruess, K., Oldenburg, C., 1999. TOUGH2 User's Guide Version 2. Lawrence Berkeley (Retrieved from) http://escholarship.org/uc/item/4df6700h.pdf.
Pruess, K., 1985. A practical method for modeling fluid and heat flow in fractured porous media. Soc. Pet. Eng. J. 25 (01), 14–26, http://dx.doi.org/10.2118/10509-PA.
Renshaw, C.E., 1995. On the relationship between mechanical and hydraulic apertures in rough-walled fractures. J. Geophys. Res.: Solid Earth 100 (B12), 24629–24636, http://dx.doi.org/10.1029/95jb02159.
Rutqvist, J., Tsang, C.-F., 2003. Analysis of thermal–hydrologic–mechanical behavior near an emplacement drift at Yucca Mountain. J. Contam. Hydrol. 62, 637–652, http://dx.doi.org/10.1016/S0169-7722(02)00184-5.
Rutqvist, J., Wu, Y.-S., Tsang, C.-F., Bodvarsson, G., 2002. A modeling approach for analysis of coupled multiphase fluid flow, heat transfer, and deformation in fractured porous rock. Int. J. Rock Mech. Min. Sci. 39 (4), 429–442, http://dx.doi.org/10.1016/S1365-1609(02)00022-9.
Rutqvist, J., Barr, D., Datta, R., Gens, A., Millard, A., Olivella, S., Tsang, Y., 2005. Coupled thermal–hydrological–mechanical analyses of the Yucca Mountain drift scale test—comparison of field measurements to predictions of four different numerical models. Int. J. Rock Mech. Min. Sci. 42 (5), 680–697, http://dx.doi.org/10.1016/j.ijrmms.2005.03.008.
Rutqvist, J., Freifeld, B., Min, K.-B., Elsworth, D., Tsang, Y., 2008. Analysis of thermally induced changes in fractured rock permeability during 8 years of heating and cooling at the Yucca Mountain drift scale test. Int. J. Rock Mech. Min. Sci. 45 (8), 1373–1389, http://dx.doi.org/10.1016/j.ijrmms.2008.01.016.
Rutqvist, J., 2008. Analysis of Injection-induced Micro-Earthquakes in a Geothermal Steam Reservoir, the Geysers Geothermal Field. Lawrence Berkeley National Laboratory, California (Retrieved from) http://eprints.cdlib.org/uc/item/4qg7v6qz.pdf.
Sarmiento, Z.F., 1986. Waste water reinjection at tongonan geothermal field: results and implications. Geothermics 15 (3), 295–308, http://dx.doi.org/10.1016/0375-6505(86)90106-9.
Settari, A., Mourits, F.M., 1998. A coupled reservoir and geomechanical simulation system. SPE J. 3 (03), 219–226, http://dx.doi.org/10.2118/50939-PA.
Settari, A., Walters, D.A., 2001. Advances in coupled geomechanical and reservoir modeling with applications to reservoir compaction. SPE J. 6 (03), 334–342, http://dx.doi.org/10.2118/74142-PA.
Stefansson, V.-đur., 1997. Geothermal reinjection experience. Geothermics 26 (1), 99–139, http://dx.doi.org/10.1016/S0375-6505(96)00035-1.
Taron, J., Elsworth, D., Min, K.-B., 2009. Numerical simulation of thermal-hydrologic-mechanical-chemical processes in deformable, fractured porous media. Int. J. Rock Mech. Min. Sci. 46 (5), 842–854, http://dx.doi.org/10.1016/j.ijrmms.2009.01.008.
Wan, J., Durlofsky, L.J., Hughes, T.J.R., Aziz, K., 2003. Stabilized finite element methods for coupled geomechanics—reservoir flow simulations. In: SPE Reservoir Simulation Symposium. Society of Petroleum Engineers, http://dx.doi.org/10.2118/79694-MS.
Wang, S., Xiong, Y., Winterfeld, P., Zhang, K., Wu, Y.-S., 2014. Parallel simulation of thermal-hydrological-mechanic (THM) processes in geothermal reservoirs. In: Proceedings of the 39th Workshop on Geothermal Reservoir Engineering, Stanford University, Stanford, California.
Wang, S., 2015. Numerical Study of Thermal-Hydraulic-Mechanical Behavior of Fractured Geothermal Reservoirs. School of Mines, Colorado.
Warren, J.E., Root, P.J., 1963. The behavior of naturally fractured reservoirs. Soc. Pet. Eng. J. 3 (03), 245–255, http://dx.doi.org/10.2118/426-PA.
Witherspoon, P.A., Amick, C.H., Gale, J.E., Iwai, K., 1979. Observations of a potential size effect in experimental determination of the hydraulic properties of fractures. Water Resour. Res. 15 (5), 1142–1146, http://dx.doi.org/10.1029/WR015i005p01142.
Witherspoon, P.A., Wang, J.S.Y., Iwai, K., Gale, J.E., 1980. Validity of cubic law for fluid flow in a deformable rock fracture. Water Resour. Res. 16 (6), 1016–1024, http://dx.doi.org/10.1029/WR016i006p01016.
Wu, Y., Di, Y., Kang, Z., Fakcharoenphol, P., 2011. A multiple-continuum model for simulating single-phase and multiphase flow in naturally fractured vuggy reservoirs. J. Pet. Sci. (Retrieved from) http://www.sciencedirect.com/science/article/pii/S0920410511001021.
Xu, T., Sonnenthal, E., Spycher, N., Pruess, K., 2006. TOUGHREACT—a simulation program for non-isothermal multiphase reactive geochemical transport in variably saturated geologic media: applications to geothermal injectivity and CO_2 geological sequestration. Comput. Geosci. 32 (2), 145–165, http://dx.doi.org/10.1016/j.cageo.2005.06.014.
Yoshinaka, R., Yoshida, J., Arai, H., Arisaka, S., 1993. Scale effects on shear and deformability of rock joints. In: Proceedings of Symposium of Scale Effects in Rock Masses (pp. 143–149), Rotterdam.
Zimmerman, R.W., Chen, G., Hadgu, T., Bodvarsson, G.S., 1993. A numerical dual-porosity model with semianalytical treatment of fracture/matrix flow. Water Resour. Res. 29 (7), 2127–2137, http://dx.doi.org/10.1029/93WR00749.
van Heel, A.P., Boerrigter, P.M., van Dorp, J.J., 2008. Thermal and hydraulic matrix-fracture interaction in dual-permeability simulation. SPE Reserv. Eval. Eng. 11 (04), 735–749, http://dx.doi.org/10.2118/102471-PA.